Check for updates

*Advanced Quantum Technologies*

ADVANCED QUANTUM TECHNOLOGIES
www.advquantumtech.com

RESEARCH ARTICLE OPEN ACCESS

# A Rack-Integrated and Modular GaAs Quantum Dot Source of Highly Entangled Photon Pairs

Yared G. Zena[1] | Moritz Langer[1] | Ahmad Rahimi[1] | Sai Abhishikth Dhurjati[1] | Pavel Ruchka[2] | Sara Jakovljevic[1,2] | Mandira Pal[1] | Frank H. P. Fitzek[3] | Harald Giessen[2] | Juergen Czarske[4] | Riccardo Bassoli[1,5] | Caspar Hopfmann[5]

[1]Institute for Emerging Electronic Technologies, IFW Dresden, Dresden, Germany | [2]4th Physics Institute and Research Center SCoPE, University of Stuttgart, Stuttgart, Germany | [3]Deutsche Telekom Chair of Communication Networks, Dresden University of Technology, Dresden, Germany | [4]Chair of Measurement and Sensor Systems Technique, TU Dresden, Dresden, Germany | [5]Quantum Communication Networks research group, Deutsche Telekom Chair of Communication Networks, Dresden University of Technology, Dresden, Germany

**Correspondence:** Caspar Hopfmann (caspar_arndt.hopfmann@tu-dresden.de)

**Received:** 24 April 2026 | **Revised:** 29 September 2026 | **Accepted:** 1 October 2026

**Keywords:** entanglement | quantum engineering | quantum light source | quantum networks | system development

## ABSTRACT

Entangled photon pair sources are a key enabling technology for quantum communication and networking, yet their deployment beyond laboratory environments is hindered by system-level complexity, limited operational stability, and insufficient industry compatibility. Here, we demonstrate a rack-based, mobile quantum light source architecture based on a semiconductor quantum dot emitter that directly addresses these challenges through modular system integration and automated quantum state verification. The source generates polarization-entangled photon pairs with an entanglement negativity $2n$ of up to $0.98 \pm 0.01$, confirming near-maximal entanglement quality. In continuous, hands-off operation over a 6 h time window, the system achieves an average combined exciton and biexciton single-photon count rate of $697 \pm 8$ kHz and a maximum rate of $740 \pm 7$ kHz, while maintaining a $2n$-value of more than 95%. These results are enabled by the integration of optical excitation, collection, cryogenic operation, and control electronics within a standardized rack footprint, together with automated monitoring. By demonstrating simultaneously high entanglement quality, sustained brightness over a 6 h period, and inherent architectural robustness in an industry-aligned system, this work advances semiconductor quantum dot devices toward deployable entangled photon sources for applied quantum photonics.

## 1 | Introduction

Quantum communication is essential for quantum information exchange between distant communication network nodes, thereby enabling key applications such as physically secure information exchange and distributed quantum computing [1, 2]. While early systems focused on simple two-node links between a sender (Alice) and a receiver (Bob), recent advances have extended this to multi-node entanglement-based quantum network architectures [3–7].

Efforts to improve compactness and modularity have also led to significant progress in using quantum technologies in field environments [8–10], such as satellite-based quantum communication systems [11] and mobile quantum communication links [12, 13] based on spontaneous parametric down-conversion

[Correction added on October 26, 2026, after first online publication: The copyright line was changed.]

This is an open access article under the terms of the Creative Commons Attribution License, which permits use, distribution and reproduction in any medium, provided the original work is properly cited.
© 2026 The Author(s). Advanced Quantum Technologies published by Wiley-VCH GmbH.

sources of entangled photon pairs. Although such sources are relatively straightforward to implement using non-linear optical techniques, their performance is ultimately constrained by their inherent Poissonian photon-number statistics [14]. In order to realize deterministic quantum communication schemes, quantum light sources are therefore indispensable. Over the past decade, great progress has been made on the field of efficient and compact single photon sources using quantum emitters [15–20]. By integrating these sources into testbeds and optical distribution systems, the vision of large-scale quantum communication and specifically quantum key distribution networks has been brought closer to reality [21–25].

To build multipartite quantum information-exchange networks and quantum-repeater architectures for future quantum networks beyond point-to-point connections, it is necessary to use on-demand entangled multi-photon sources that are highly efficient, feature close to unity entanglement fidelities and high indistinguishabilities [23, 26–29]. Notably, the exciton-biexciton cascade in GaAs quantum dots (QDs) provides a highly efficient mechanism for entangled-photon pair emission, positioning these systems as leading candidates for on-chip entangled photon sources [30–38].

Despite substantial progress in source physics and optical performance, the majority of demonstrated entangled photon sources remain confined to laboratory environments and are not readily deployable in applied or industrial contexts. This gap between laboratory demonstrations and field-ready systems is not primarily limited by entanglement quality or single-photon purity, but rather by system-level challenges. These include the need for Continuous manual alignment, limited operational stability, bespoke experimental setups and layouts, and tight coupling between optical performance and strict environmental controls, such as temperature and vibrational stability. As a result, state-of-the-art entangled photon sources are difficult to operate reliably outside controlled laboratory settings, hindering their adoption in emerging quantum communication network demonstrators that demand long-term, autonomous, and reproducible operation in industrial environments such as server rooms.

In parallel, applied quantum photonics has begun to place increasing emphasis on deployment-oriented metrics, such as operational uptime, automation, footprint, and system interoperability [39, 40]. For entangled photon sources to transition from experimental platforms to enabling infrastructure, their design must explicitly account for these requirements at the architectural level, rather than treating them as secondary engineering considerations.

Toward the goal of industrial deployment of high-performance quantum systems based on GaAs QDs, significant progress has been made by developing fiber-based platforms. Fiber-coupled source systems integrated into cryogenic environments below 10 K are necessary to attain high-performance devices within a small footprints. Such systems have demonstrated reliable and scalable operation, providing a pathway toward practical and commercial deployment. Notable advancements include the development of efficient single photon sources [18, 41], indistinguishable single photons [42], fiber-pigtailed, integrated sources [43], GHz-clocked entangled photon pair sources based on QDs [34, 44], and ultra-compact, fiber-coupled single and entangled photon pair sources using 3D-printed micro-objectives [45, 46]. Additionally, techniques for collecting telecom-wavelength photons from circular Bragg gratings with optical fibers and 3D-printed microlenses have been demonstrated [47]. Together, these approaches represent a robust foundation for high-performance, fiber-integrated quantum photonic devices for semiconductor QDs suitable for industrial applications. In this work, we address this challenge by developing and experimentally validating a rack-based, mobile entangled photon source built around a semiconductor GaAs QD emitter. Rather than optimizing a single performance metric in isolation, our approach focuses on system-level integration and operational robustness, while retaining near-ideal entanglement quality. Recent studies demonstrate that relevant performance indicators for industrial quantum networks are the temporal stability of three key parameters: the photon-pair generation rate, the indistinguishability of the emitted photons, and the entanglement fidelity [43, 48]. To frame this approach, we operationally define *industrial compatibility* of an entangled photon source through the following system-level properties:

- **Standardized footprint**: integration within 19-inch rack enclosures, compatible with existing industrial infrastructures, such as server rooms and fiber network nodes.
- **Continuous** operation: closed-loop stabilization of optical alignment, excitation conditions, and polarization settings, with a target autonomous operation time exceeding 24 h without manual intervention.
- **Operational stability**: sustained entangled photon generation with less than 5% drift in key performance metrics (brightness, fidelity) over the autonomous operation time period.
- **Remote accessibility**: full software-based control and monitoring via standardized communication interfaces, enabling unattended and geographically distributed operation.
- **Deployability**: vibration and thermal robustness compatible with relocation without permanent degradation of source performance.

These criteria translate the often qualitative notion of deployability into concrete, testable system requirements and form the design rationale for the architecture presented in this manuscript. Furthermore, these engineering goals are general in nature and extend beyond the specific system described in this work. While achieving near-unity indistinguishability is indispensable for entangled photon sources in future interference-based multipartite networks [49], it is not the primary figure of merit for a standalone source system. Consequently, its optimization is deferred to future implementations.

While fully satisfying this framework remains an ongoing engineering target, we demonstrate significant progress toward these goals by generating polarization-entangled photon pairs with an entanglement negativity $2n$ of up to $0.98 \pm 0.01$. Moreover, we show sustained and hands-off operation over a 6 h time window with an average single-photon emission rate of $697 \pm 8$ kHz (fluctuating by less than 15%) while maintaining a $2n$-value



25119044, 2026, 10, Downloaded from https://advanced.onlinelibrary.wiley.com/doi/10.1002/qute.70510 by Universitatsbibliothek Stuttgart, Wiley Online Library on [02/11/2026]. See the Terms and Conditions (https://onlinelibrary.wiley.com/terms-and-conditions) on Wiley Online Library for rules of use; OA articles are governed by the applicable Creative Commons License

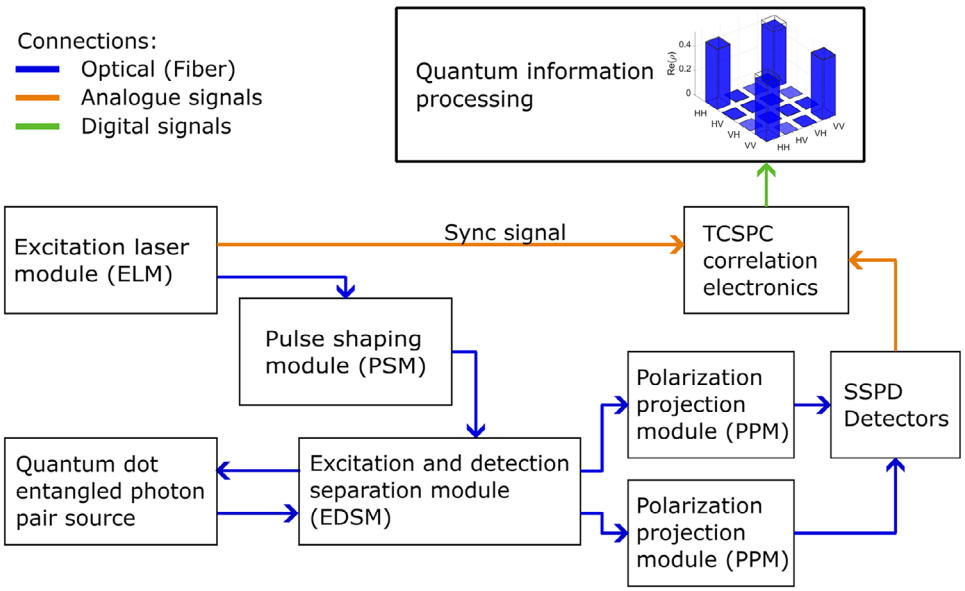



**FIGURE 1** | High-level schematic overview of the compact, industry-compatible entangled photon pair source system architecture housed within 19-inch rack systems. The principles and design considerations of the various modules are discussed in the text.

exceeding 95%. These results are obtained in a fully integrated, rack-based system incorporating optical excitation and collection, cryogenic operation, and automated data collection and analysis infrastructure.

The remainder of this work is structured as follows. Beyond the system requirements and design rationale derived from the industrial compatibility criteria outlined in this section, Section 2 discusses the system design and illustrates the architecture and implementation of the rack-based quantum dot entangled photon pair source system. In Section 3, the entangled photon pair source with in situ fiber coupling of the quantum dot inside a compact cryostat is discussed. This is followed by Section 4 in which experimental results validating entanglement quality, brightness, and long-term stability are presented. Finally, Section 5 concludes the manuscript. The provided in Supporting Information[1] detail additional information, including experimental apparatus, exciton fine-structure splitting, correlation tomography, and exciton lifetime.

## 2 | System Design and Implementation

The entangled photon pair source system presented in this work incorporates all the required hardware to operate the source. As illustrated in Figure 1, this includes the cryogenically cooled GaAs QD emitter, the excitation laser system, all optics, polarization projection, the superconducting single-photon detector (SSPD) system, the time-correlated single-photon counting (TCSPC) electronics, the computer-based quantum information processing as well as the automated control system. The basic working principle of this entangled photon pair source follows that of previous successful laboratory-based demonstrations of such systems [34, 46].

Contrary to these previous laboratory-based entangled photon pair system realizations, the source system presented here is designed and implemented completely within two industry-standard 600 mm-wide, mobile 19-inch racks on wheels, as schematically illustrated in Figure 2. This modular architecture allows compact integration of all components while maintaining flexibility for system modifications. Interconnections within each rack and between the two racks are realized via electrical cables and low-loss single mode optical fibers, ensuring reliable signal routing and minimal transmission losses. Due to these premises, the free-space optical excitation and detection of the QD-source inside the cryostat and therefore the employment of direct in situ fiber coupling of the QD output signal, as established in Ref. [46], becomes indispensable.

One rack is primarily dedicated to housing the QD-chip as well as the SSPDs each within closed-cycle cryostats. The fiber-coupled QD-chip constituting the entangled photon source is placed within a Attocube 800XS cryostat from Attocube Systems GmbH. The employed SSPDs system is commercial system with a nominal timing resolution of 20 ps (root-mean-square) and 85% efficiency from Single Quantum. The two rack-mountable He-compressors required for the cryogenic operation (IGLU from Attocube Systems GmbH) are placed next to the cryogenic systems rack.

The second rack system is dedicated to the optical modules and therefore contains all optical instrumentation required for the operation of the entangled-photon pair source. This includes the excitation laser source, wavelength filtering optics, polarization projection units, and vibration dampening system. A detailed description of the employed systems and devices are given in the following and in the Supporting Information.[1]

All optical systems are subdivided into compact modules which consist of 400 mm × 600 mm Aluminum breadboards. These modules are placed on rubber vibration isolation pads in drawers of 4 U[2] height mounted within the rack. This approach facilitates both access for fine-tuning of the optics while retaining a compact



25119044, 2026, 10, Downloaded from https://advanced.onlinelibrary.wiley.com/doi/10.1002/qute.70510 by Universitatsbibliothek Stuttgart, Wiley Online Library on [02/11/2026]. See the Terms and Conditions (https://onlinelibrary.wiley.com/terms-and-conditions) on Wiley Online Library for rules of use; OA articles are governed by the applicable Creative Commons License

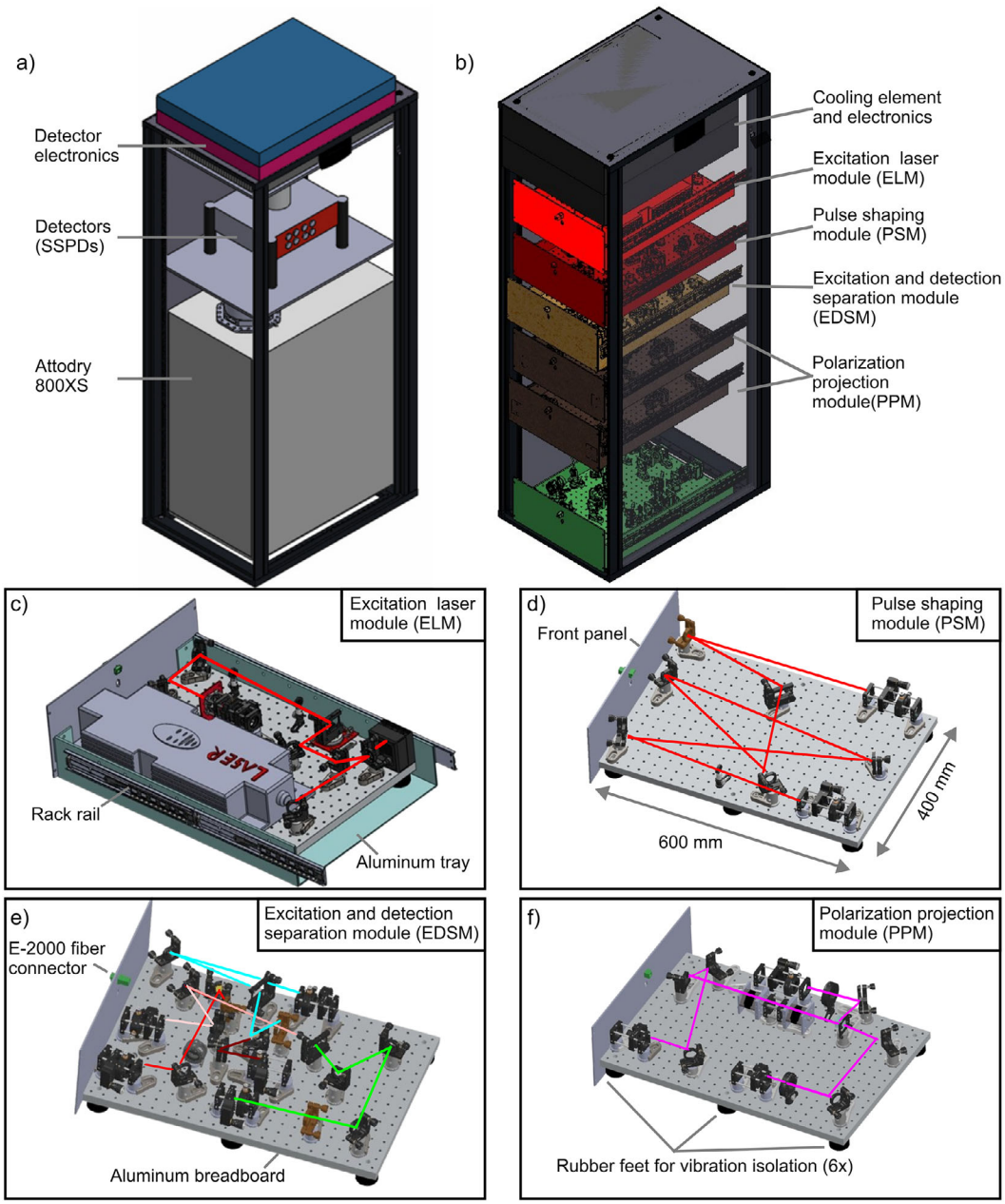



**FIGURE 2** | Illustration of the rack-based quantum dot entangled photon pair source system architecture. (a) Source cryostat and detection rack: Contains the cryostat system together with the associated electronics for the GaAs quantum dot source and single photon time-resolved detection. (b) The optics rack system contains the modular optical subsystems: (c) excitation laser module (ELM), which features a pulsed (Ti:Sa) laser system operating at a 1 GHz repetition rate, (d) pulse shaping module (PSM), (e) excitation and detection separation module (EDSM), and two (f) automated polarization projection modules (PPMs). The optics rack also integrates the Ti:Sa laser controller, motor controllers, and cooling electronics, all of which are fully integrated into this rack. The excitation laser, X and XX detection paths are illustrated as red, blue and green lines, respectively. The purple line indicates either a X or XX detection path. A detailed description of the optical layout of each module is given in the Supporting Information[1].

footprint while in operation. For optical in- and outputs of the modules low-loss E2000 fiber connectors in conjunction with 780 nm single mode active core-aligned fibers (from Diamond SA) are used, which feature losses < 0.2 dB per connector. This approach ensures minimal losses of the optical module interconnects. The following optical modules are employed in this work:

- Excitation laser module (ELM),
- Pulse shaping module (PSM),
- Excitation and detection separation module (EDSM),
- Two polarization projection modules (PPM).

The optical modules are mounted in a thermally isolated, fully enclosed rack system, further details are found in the Supporting Information.[1] In future iterations of this system it is planned to stabilize the temperature within the rack to improve the long-term stability of the system for variable environments. This active stabilization system, however, is not used in this work. Indirect



25119044, 2026, 10, Downloaded from https://advanced.onlinelibrary.wiley.com/doi/10.1002/qute.70510 by Universitatsbibliothek Stuttgart, Wiley Online Library on [02/11/2026]. See the Terms and Conditions (https://onlinelibrary.wiley.com/terms-and-conditions) on Wiley Online Library for rules of use; OA articles are governed by the applicable Creative Commons License

temperature stability is provided by the laboratory climate control system, which nominally provides stabilization of the ambient temperatures to 18°C ± 2°C.

The QD optical excitation is provided by a GHz-clocked, 40 fs pulsed width Ti:Sa laser system (Novanta Taccor Tune). This laser system output features a spectral bandwidth of 14 nm which is filtered within the ELM using a transmission grating (1200 l/mm, 800 nm blaze) down to a spectral full width half maximum (FWHM) of 0.35 nm before coupling it to a polarization-maintaining single mode fiber. In order to further reduce the spectral bandwidth and improve the signal to background ratio, the excitation signal is filtered in the PSM using another transmission grating to a FWHM of 0.1 nm.

The excitation beam first passes through a computer-controlled rotating half-wave plate, followed by a fixed linear polarizer, which together control the intensity of the excitation laser entering the cryostat, as shown in Figure 2c and in the Supporting Information.[1] The filtered excitation signal is fed into the EDSM, in which it is overlaid with the output signal of the QD and sent to the QD using a volume Bragg grating notch filter of 0.4 nm bandwidth tuned to the excitation wavelength as a spectrally selective mirror. Entangled photon pairs are created from the GaAs QD using the established process of two-photon excitation of the QD biexciton state $|XX\rangle$ [50], see Section 4 for further details. The resulting polarization entangled QD exciton (X) and biexciton (XX) photon signals are separated and filtered in the EDSM into respective output signals. The optical efficiency from the cryostat fiber coupler to the X and XX detection path couplers is about 30%, limited by multiple stages of notch and transmission grating filters. These X and XX output signals constitute the core of the entangled photon pair source and can, in future uses of the presented system, be employed as a core building block of quantum communication networks. In presented implementation, the X and XX output signals are directed to two separate PPMs. In these modules, the X and XX photons are projected using computer-controlled combination of half- and quarter-zero-order waveplates before a polarizing beamsplitter. This system enables the projection onto the linear (H/V), diagonal (D/A) and circular (R/L) polarization directions, cf. Section 4 and our previous publications [34, 46]. The projected photons are detected using the rack-based SSPD system, the outputs of which are collected as time- and channel-resolved single photon detection events using commercial time tagger electronics (TimeTagger Ultra from Swabian Instruments GmbH). Using hardware-accelerated software-based processing, the event data is turned into time-correlated single photon counting (TCSPC) signals, which are processed further in order to extract the time- and polarization-resolved two-photon correlation required to determine the two-photon density matrix of the source in a given time frame.

## 3 | Entangled Photon Pair Source

The key component of entangled photon pair sources are optically driven and coupled GaAs QDs. These QDs are embedded in a $Al_xGa_{1-x}As$ heterostructure grown by molecular beam epitaxy (MBE) using in situ liquid droplet etching and subsequent infilling of nanoholes [51–53]. Millimeter-sized nanomembranes with embedded QDs are released and transferred to a gold-coated GaAs wafer before processing with gray-scale lithography into monolithic microlenses. The manufacturing process of the monolithic microlenses with embedded QDs is detailed in Ref. [38] and further details on the employed heterostructure and growth process are given in the Supporting Information.[1] It is important to note that the QDs within the monolithic microlenses are statistically rather than deterministically positioned. Consequently, about every 200th microlens functions as a bright entangled photon pair source [38]. To ensure ample supply of high-performance entangled photon pair sources, large arrays of QD-microlenses are fabricated, cf. Figure 3.

Due to the working principle of these quantum emitters, cryogenic cooling to temperatures below 10 K is indispensable [50, 53]. To transition these sources from laboratory environments to deployable systems, in situ coupling to single-mode fibers is essential. Earlier implementations of in situ fiber coupling relied on fixed-glue assemblies [20, 54–56], which provide no free mechanical alignment once cured, and restrict operation to a single QD. While simple, this approach is highly sensitive to thermal strain, especially because device preparation is done at room temperature while measurements are carried out in cryogenic environments. As a result, such fiber coupling approaches often exhibit limited brightness, are not reconfigurable, and typically allow only a limited number of cooling cycles. In the presented work, we extend our previous work on compact entangled photon pair sources using monolithic QD-microlenses in situ coupled to single-mode fibers with 3D-printed micro objectives [38, 46] to a more compact cryostat geometry and optical system implementation compatible with 19-inch rack systems. This approach avoids the limitations of glue-fixed assemblies and enables reproducible alignment under cryogenic conditions. Finite-difference time-domain simulations of this in situ optical collection approach indicate that a coupling efficiency between QD emission and single mode fiber of up to 37% is achievable if the realized 3D-morphology measured by atomic force microscopy of the fabricated QD-microlenses is taken in account [38, 46]. The experimentally achieved coupling efficiency of the QD emission into the single mode fiber is practically not readily accessible, a detailed discussion is found in the Supporting Information.[1]

A strain-relief system consisting of an Aluminum block with a 1 mm hole drilled at 45° is mounted vertically on the side of the lens holder. By gluing the Acrylate-coated fiber into this block using UV-activated adhesive, the mechanical stress on the fragile, bare lensed fiber tip is minimized. Further details are found in Ref. [46].

The QD-chip is mounted on a XY translation stage beneath the fiber, enabling lateral scanning and allowing individual microlenses to be addressed as needed. Additionally, a $z$-axis stage is used to control the distance between the fiber and the QD-chip, see illustration in Figure 3a. The optimal focus distance between fiber micro objective and QD-chip is about 35 µm, illustrating the compact nature of the arrangement, cf. Figure 3b. Figure 3c shows an optical microscopy image of the monolithic QD-microlens sample utilized in this work, the fabrication process of these devices is detailed in Ref. [38]. Figure 3d presents a scanning electron microscopy (SEM) image, recorded at a 45° tilt, depicting an array of monolithic $Al_{0.15}Ga_{0.85}As$ QD-microlenses fabricated on a gold-coated GaAs substrate.



25119044, 2026, 10, Downloaded from https://advanced.onlinelibrary.wiley.com/doi/10.1002/qute.70510 by Universitatsbibliothek Stuttgart, Wiley Online Library on [02/11/2026]. See the Terms and Conditions (https://onlinelibrary.wiley.com/terms-and-conditions) on Wiley Online Library for rules of use; OA articles are governed by the applicable Creative Commons License

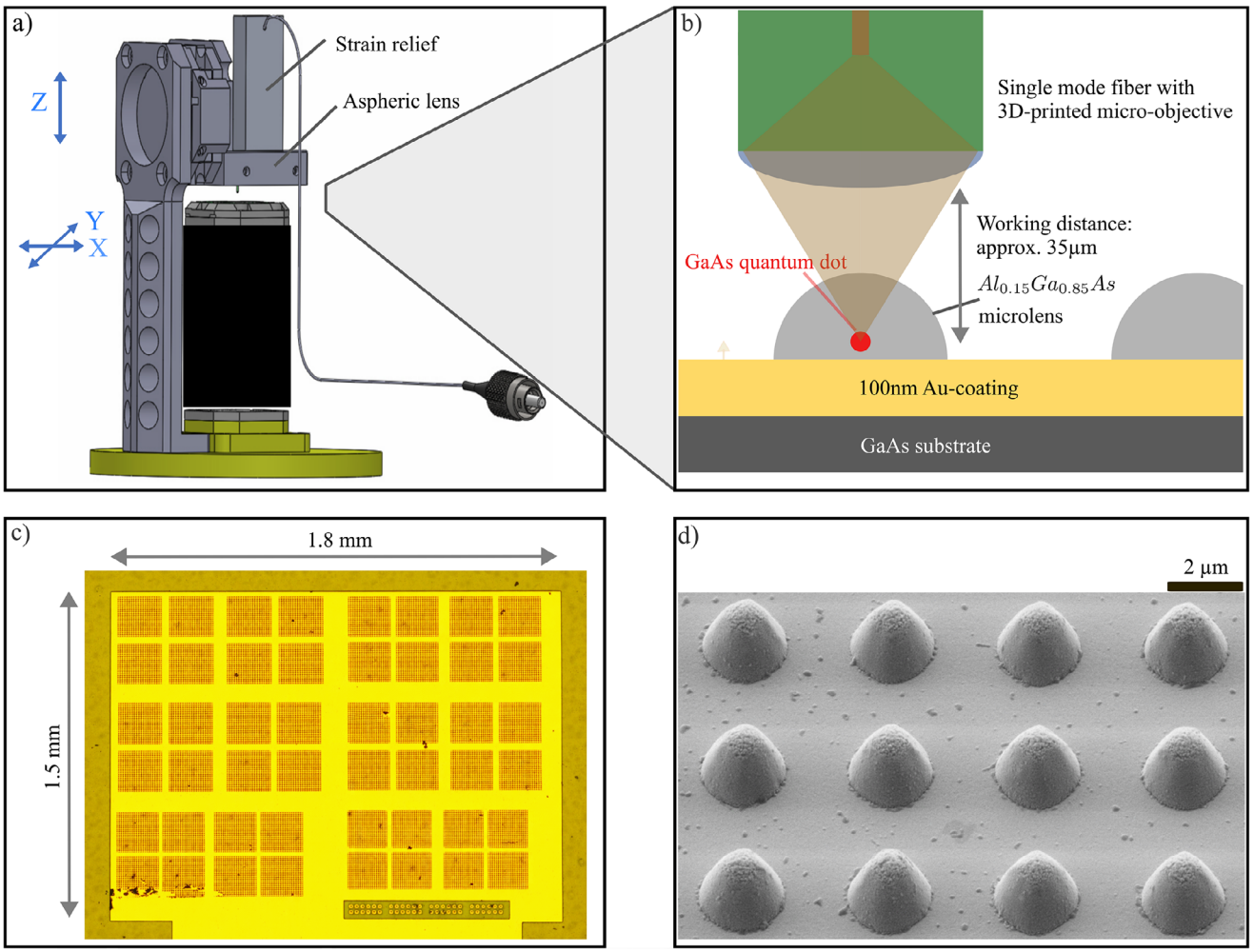



**FIGURE 3** | Overview of the employed approach of in situ fiber-coupling of entangled photon pairs sources based on GaAs quantum dots embedded in $Al_{0.15}Ga_{0.85}As$ monolithic microlenses. (a) Three-dimensional representation of the cryostat interior design of the in situ fiber coupling system, which includes the fiber-strain-relief unit and free-space-accessible lens for coarse alignment of the fiber micro-objective. Alignment directions for the QD to fiber collection using piezo driven stages (X,Y,Z) are indicated by blue arrows. (b) Illustration of the QD-microlens emission collection into a 3D-printed micro objective attached to a single mode fiber. (c) A microscopy picture of the monolithic QD-microlens sample chip used in this study. Its dimensions are 1.8 × 1.5 mm, featuring 19200 lenses arranged in 48 fields of 20 × 20 lenses. (d) Scanning electron micrograph under a 45° tilt.

This compact design is integrated into the cryogenic system, as shown in Figure 2a, and is connected to the optical rack via a single mode fiber. This arrangement mechanically decouples the optical system from the cryogenic environment, significantly improving its robustness - especially outside well-controlled laboratory environments. Consequently, both the footprint and complexity of the optical and optoelectronic subsystems are significantly reduced, optimizing the use of available space and simplifying the overall setup. The optical connection is implemented using a single-mode fiber terminated with low-loss connectors, providing reliable, efficient coupling of the quantum light source to the optical system.

## 4 | Results and Discussion

To assess the practical usability of the optical system developed in section Section 2, it is essential to evaluate its optical performance under realistic operating conditions. For this purpose, a series of experimental measurements are carried out. In order to find QDs in microlenses suitable as entangled photon pair sources on the sample chip, above-band photoluminescence spectroscopy is performed. The employed apparatus is presented in the Supporting Information.[1] Criteria for the suitability of QDs for the purpose of entangled photon pair sources are predominately high brightness, exciton emission wavelength within 778–781 nm and low fine-structure splitting $\Delta_{FSS}$. After investigating 16 QD-microlenses in this wavelength range, the best QD candidate is identified, cf. Figure 4a. Further details on the selection process are given in the Supporting Information.[1] All subsequent experimental results shown in this work are obtained on this specific QD.

To utilize the QD as a deterministic entangled photon pair source, pulsed resonant two-photon excitation (TPE) is employed [30, 57]. This excitation approach enables coherent resonant pumping of the $|XX\rangle$ state through the simultaneous absorption of two photons, which consequently undergoes a cascaded radiative decay that produces two photons, one from the $|XX\rangle \rightarrow |X\rangle$ transition and one from the $|X\rangle \rightarrow$ ground-state $|0\rangle$ transition [30, 57], cf. Figure 4b. Because angular momentum is conserved[3]



25119044, 2026, 10, Downloaded from https://advanced.onlinelibrary.wiley.com/doi/10.1002/qute.70510 by Universitatsbibliothek Stuttgart, Wiley Online Library on [02/11/2026]. See the Terms and Conditions (https://onlinelibrary.wiley.com/terms-and-conditions) on Wiley Online Library for rules of use; OA articles are governed by the applicable Creative Commons License

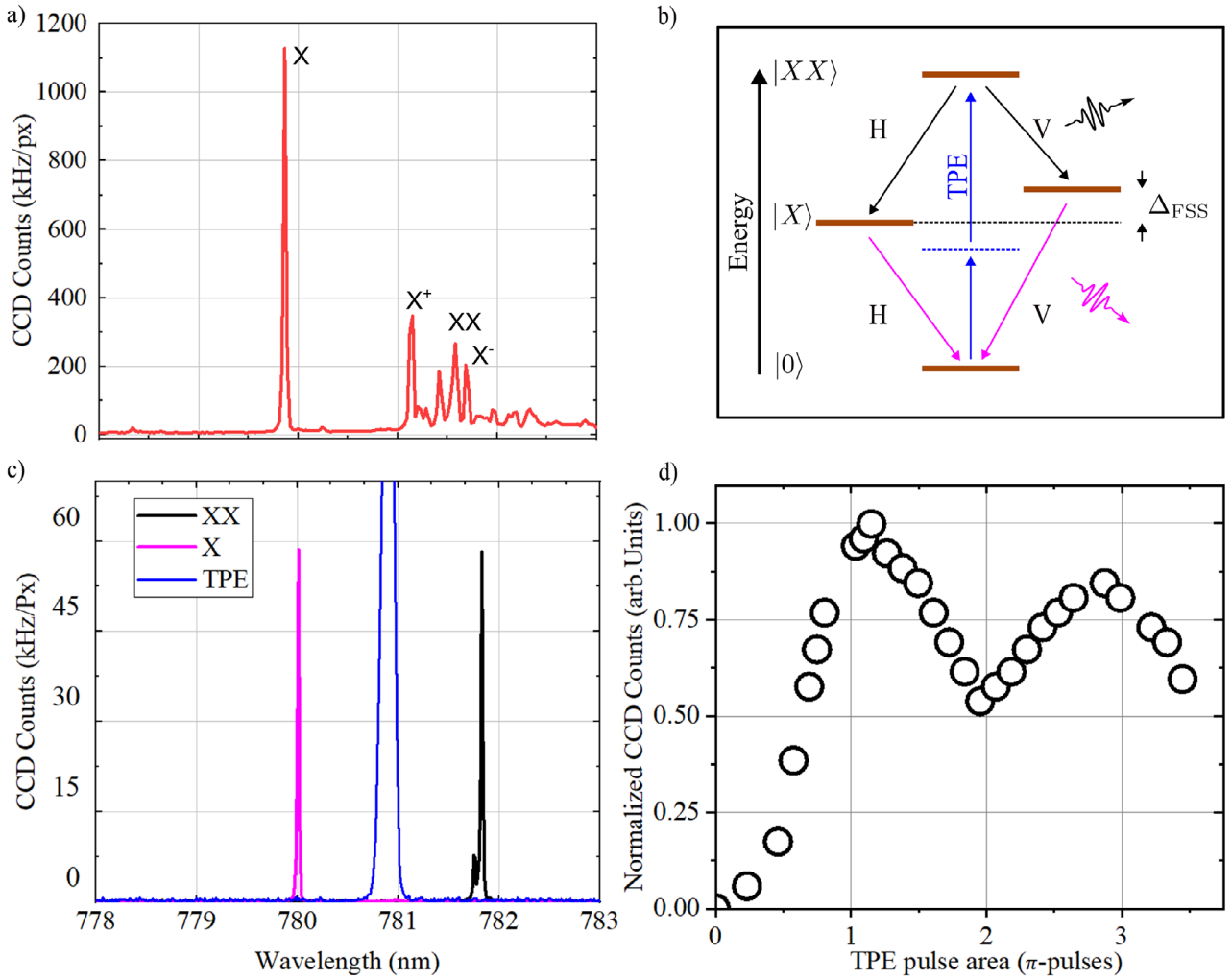



**FIGURE 4** | (a) Above-band excitation spectrum of a single GaAs QD-microlens captured using a 3D-printed objective on top of a single-mode fiber. The exciton (X), biexciton (XX), negative and positive trion ($X^-$ and $X^+$) QD emission lines are annotated. (b) Schematic illustration of the two-photon resonant excitation (TPE) and entangled photon pair creation scheme. (c) Micro-photoluminescence spectrum of the selected QD under two-photon excitation at the $\pi$-pulse excitation. The $|XX\rangle \rightarrow |X\rangle$ and the $|X\rangle \rightarrow |0\rangle$ emission lines are shown in black and pink, respectively. (d) Normalized CCD count rate as a function of TPE pulse area. The first Rabi $\pi$-pulse is achieved at an average power of 9 μW at a laser repetition rate of 1 GHz.

throughout these two sequential spontaneous emission events, the emitted photon pairs are polarization-entangled. Owing to the coherent nature of the TPE excitation process, the population of the $|XX\rangle$ state exhibits Rabi oscillations that depend on the excitation pulse power, cf. Figure 4d. It can therefore be used to realize deterministic QD-entangled photon pair sources by using the first Rabi $\pi$-pulse achieved at an average excitation power of 9 μW. This corresponds to a per-pulse energy of 9 fJ. Due to the finite $\Delta_{FSS}$ of the $|X\rangle$ state, polarization state precession oscillations are induced, this effect is discussed in detail in Refs. [34, 58]. For the quantum dot studied here, the fine-structure splitting $\Delta_{FSS}$ is determined using polarization resolved PL-spectroscopy to 2.54(12) μeV. Details on the experimental derivation of this value is found in the Supporting Information.[1] A energetic shift ($\Delta E \simeq 0.3$ meV) of the X and XX optical transitions is observed when TPE is employed versus above-band excitation, see Figure 4a,c. This effect can be attributed to charge traps in the vicinity of the QD that can influence the QD energetic states via the quantum-confined Stark effect. The occupation of these defects in turn is dependent on the conduction and valence band carrier densities and therefore on the excitation scheme [59, 60]. In Figure 4c emission of a parasitic QD transition, likely a spin-blockaded positive trion $X^+$ [61], is observed close to the XX transition. This transition originates from the excitation of the $|X^+\rangle$ state due to unwanted phonon-assisted resonant excitation at the TPE excitation energy [62], cf. Figure 4a,c. For the observation of entanglement properties via time-resolved two-photon correlation spectroscopy this parasitic emission is not relevant as only cascaded events within both X and XX spectral detection windows contribute significantly to these measurements.

To reconstruct the two-photon density matrix of the entangled state, a full polarization tomography by measuring time-resolved X–XX coincidences across all $6 \times 6 = 36$ polarization basis combinations is performed. Using an integration time of 60 s per basis combination a complete tomography is performed in 24 min. The presented coincidence measurements, the full matrix representation of the coincidences can be found in the Supporting Information,[1] is performed by integrating five tomography itera-



25119044, 2026, 10, Downloaded from https://advanced.onlinelibrary.wiley.com/doi/10.1002/qute.70510 by Universitatsbibliothek Stuttgart, Wiley Online Library on [02/11/2026]. See the Terms and Conditions (https://onlinelibrary.wiley.com/terms-and-conditions) on Wiley Online Library for rules of use; OA articles are governed by the applicable Creative Commons License

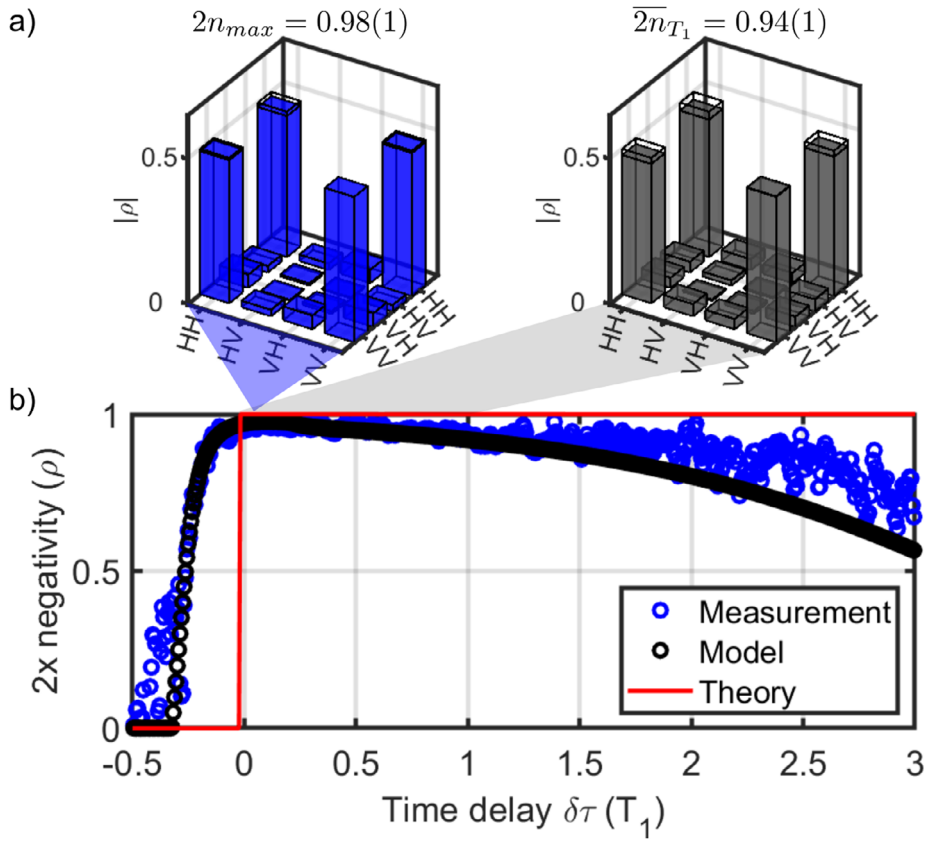



**FIGURE 5** | (a) Representation of the absolute values of two-photon density matrix $\rho$ using 1GHz-clocked two-photon resonant excitation. Both $\rho$ representations for the maximal within an 8 ps window and lifetime $T_1$-averaged entanglement negativities $2n_{max}$ and $\overline{2n}_{T_1}$, respectively, are shown. (b) $2n$ as a function of time delay $\delta\tau$ between the X-XX two-photon coincidences. The measured $\rho$ and $2n$ (blue curve) are derived from the full X-XX two-photon coincidence tomography measurement over all 36 detection polarization combinations; the full dataset is shown explicitly in the Supporting Information.[1] The green and red curves represent the calculated $2n$-values of an ideal maximally entangled model with and without considering a limited single-photon detector timing resolution, respectively.

tions corresponding to an integration time of 120 min in order to assure high statistical significance of the dataset. The two-photon density matrix reconstruction procedure follows the standard methodology described in Refs. [34, 58, 63]. As the source entanglement figure of merit the negativity of the two-photon density matrix is used, as its value is independent of rotations, contrary to the entanglement fidelity.

The time-resolved two-photon density matrix results are presented in Figure 5. Besides the experimental data shown in blue, the ideal maximally entangled theoretical model and the model with limited detector timing resolution is shown in red and black, respectively. The modeling of the maximally entangled state follows Refs. [34, 58] and is explicitly shown in the Supporting Information.[1] The assumed full-width half-maximum two-photon detector timing resolution is 50 ps. The good agreement between the experimental data and the maximally entangled state model indicates that the entangled photon pairs generated by this source closely approximate a maximally entangled state. The top panel of Figure 5 exemplary shows two-photon density matrix $|(\rho)|$ exhibiting the maximal entanglement negativity ($2n$) of 0.98(1) within an 8 ps window. The degree of entanglement is quantified using the entanglement negativity, 2n as a function of the time delay $\delta\tau$ between the XX and X photon emission events in units of the X lifetime $T_1^X$. The X lifetime is determined to a value of 162(4) ps. The weighted average $2n$-value over one $T_1^X$ equates to 0.94(1), demonstrating the highly entangled nature of the emitted photon pairs in the presented source even in the presence of finite $\Delta_{\mathrm{FSS}}$. When integrating over the full period of 1 ns, the $2n$-value is 0.89(1). Using the XX auto-correlation coincidences from the same two-photon coincidence measurement a single photon purity of 99.2(2)% of the source can be inferred, see Supporting Information.[1]

One of the important aspects for industry-compatible entangled photon pair sources is reliable, sustained performance. In order to assess this aspect in the presented source system a 6 h uninterrupted and hands-off operation is performed cf. Figure 6. Importantly, no active polarization or temperature stabilization system is used during this measurement, this enables evaluation of the system robustness in a realistic environment.

The average recorded combined X and XX single photon flux as observed in the V polarization direction is $697 \pm 8$ kHz, the flux exhibits fluctuations of less than 15%. While this variation currently exceeds our operational stability target of <5% drift, maintaining this level of performance without active stabilization demonstrates the baseline mechanical and thermal stability of the presented rack-mounted quantum light source. The maximal observed combined single photon rate is 740 kHz. Figure 5b



25119044, 2026, 10, Downloaded from https://advanced.onlinelibrary.wiley.com/doi/10.1002/qute.70510 by Universitatsbibliothek Stuttgart, Wiley Online Library on [02/11/2026]. See the Terms and Conditions (https://onlinelibrary.wiley.com/terms-and-conditions) on Wiley Online Library for rules of use; OA articles are governed by the applicable Creative Commons License

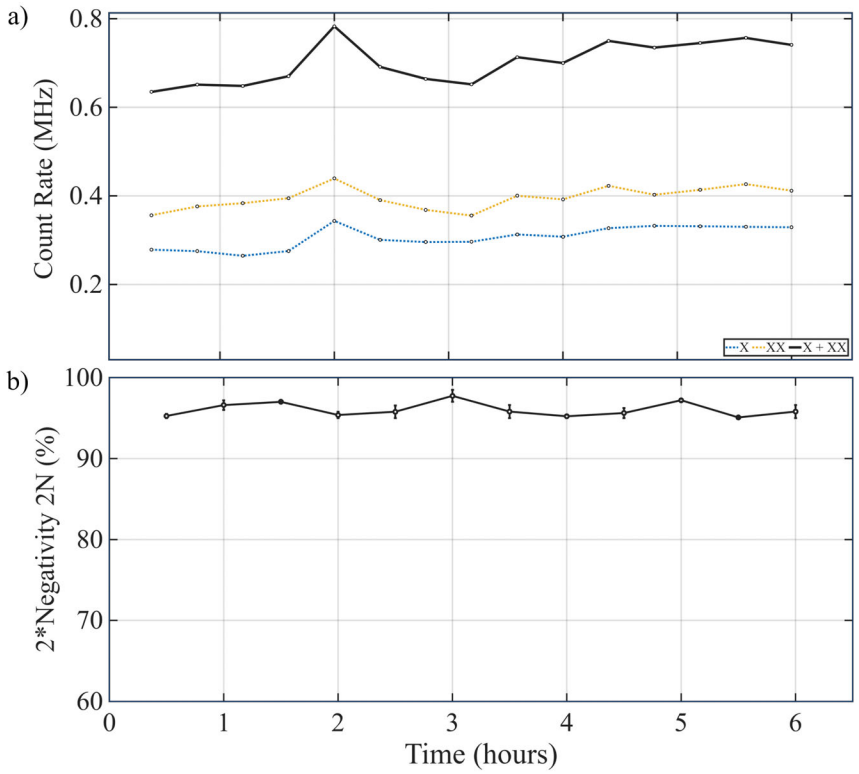



**FIGURE 6** | Unattended performance of the rack-based entangled photon pair source over a 6 h window. (a) X, XX and combined single photon detection rates collected in the V polarization basis over time. (b) Entanglement negativity $2n$ for $\delta\tau \to 0$ within an 8 ps time window, cf. Figure 5, as a function of time, error bars are indicated.

depicts the peak $2n(\delta\tau \to 0)$-value within a 8 ps coincidence window over time. The average $2n(\delta\tau \to 0)$ is 0.960(4), all observed values, however, remain above the 0.95 limit. This remarkable result demonstrates the high robustness of the presented rack-mounted quantum light source. Nevertheless, the observed fluctuations in the rates and negativity over time are due to instabilities and drifts within the entangled photon pair source system. The recorded negativity values are influenced by the stability of the polarization projection and quantum dot carrier complexes and are much less affected by optical efficiency fluctuations than the photon rates are. The observed rates are subject to the stability of the optical system and especially so on the single mode fiber couplings. The couplings are sensitive to mechanical shifts induced by vibrations and temperature changes over the measurement time.

These observations confirm that the presented ultra-compact, industrial 19-inch rack entangled photon pair source is capable of delivering consistent high-performance results over a scale of several hours without human intervention. While further long-term validation over days and weeks as well as the implementation of active stabilization mechanisms, is warranted, the presented results pave the way toward this goal and bring these sources significantly closer to practical deployment.

## 5 | Conclusions

In this work, we demonstrate a modular, rack-based entangled photon pair source architecture that bridges the gap between high-performance laboratory emitters and deployable industrial quantum infrastructure. By integrating a semiconductor GaAs quantum dot emitter within a standardized 19-inch rack footprint, we address the core requirements for industrial compatibility: portability, system-level integration, and operational autonomy. Further improvements and refinement to the presented source system are however necessary to fully meet all engineering goals.

These results validate that transitioning to a compact, fiber-coupled form factor does not necessitate a compromise in the fundamental quality of the quantum light. Through the use of monolithic $Al_{0.15}Ga_{0.85}As$ monolithic microlenses and in situ 3D-printed micro-objectives, we achieve near-ideal polarization entanglement with an entanglement negativity $2n$ of up to $0.98 \pm 0.01$ under resonant two-photon excitation. This high degree of entanglement is complemented by near-perfect multi-photon suppression, evidenced by a measured single-photon purity of 99.2% ± 0.2%. Furthermore, the system demonstrates high-rate photon emission, maintaining an average single-photon flux of $697 \pm 8$ kHz during a 6 h period of entirely unattended, hands-off operation. Crucially, the observed operational stability over the 6-hour test—characterized by $2n$ exceeding 95% and emission rate fluctuations remaining within 15%—is achieved without active temperature or polarization stabilization. This inherent mechanical and thermal robustness, facilitated by the compact and modular system design, represents a substantial step toward meeting the criteria for deployability in environments such as server rooms or network nodes. While the achieved performance characteristics do not inherently exceed previously reported values of entangled photon pair sources [32–34, 46],



25119044, 2026, 10, Downloaded from https://advanced.onlinelibrary.wiley.com/doi/10.1002/qute.70510 by Universitatsbibliothek Stuttgart, Wiley Online Library on [02/11/2026]. See the Terms and Conditions (https://onlinelibrary.wiley.com/terms-and-conditions) on Wiley Online Library for rules of use; OA articles are governed by the applicable Creative Commons License

they are very much comparable to the state-of-the-art. Realizing this in a compact, rack-based system optimized for compatibility with industrial environments represents a significant step toward the scalable utilization of these sources in future industrial and commercial quantum communication networks.

While the current demonstration confirms the feasibility of autonomous operation over several hours, future iterations will focus on implementing the outlined closed-loop stabilization and thermal management systems to extend the autonomous window beyond 24 h. By successfully housing the full quantum-optical stack—from cryogenic cooling to automated polarization projection - within a mobile, industry-aligned architecture, this work provides a scalable blueprint for the next generation of entangled photon sources required for distributed quantum communication networks.


### Acknowledgments

The authors acknowledge Yana Vaynzof and Stefan Krause for valuable discussions and suggestions. This work was funded by the Federal Ministry of Research, Technology and Space of Germany (BMFTR) projects QR.X, QR.N, QUARKS, QUIET, QD-CamNetz, and Integrated3Dprint (contracts no. 16KISQ013, 16KISQ016, 16KIS2194, 16KIS1998K, 16KISQ094, 16KISQ078, and 13N16875), German Research Foundation (DFG, grant no. 431314977/GRK2642) and DFG Reinhart Koselleck-Program (CZ 55/61-1).

Open access funding enabled and organized by Projekt DEAL.


### Conflicts of Interest

The authors declare no conflicts of interest.

### Data Availability Statement

All data that support the findings presented in this work are available from the corresponding author upon reasonable request.

### Endnotes

[1] "See Supplemental Material at [URL will be inserted by publisher] for more information on the experimental apparatus, exciton finestructure and lifetime, as well as correlation tomography," (2026).

[2] A standard rack height unit (U) corresponds to a height of 44.45 mm.

[3] Specifically, both the initial $|XX\rangle$ state and the final ground state $|0\rangle$ have a total angular momentum $j$ of zero, while the emitted photons carry angular momentum $j_\nu = \pm 1$. It follows that the spins (polarizations) of X and XX photons are quantum-correlated because $j_\nu^{XX} + j_\nu^{X} = 0$.

### References


1. P. Ball, "Jian-Wei Pan: Building the Quantum Internet," *National Science Review* 6, no. 2 (2018): 374–376, https://doi.org/10.1093/nsr/nwy102.

2. H. J. Kimble, "The Quantum Internet," *Nature* 453, no. 7198 (2008): 1023–1030.

3. S. R. Hasan, M. Z. Chowdhury, M. Sayem, and Y. M. Jang, "Quantum Communication Systems: Vision, Protocols, Applications, and Challenges," *IEEE Access* 11 (2023): 1–20, https://doi.org/10.1109/ACCESS.2023.3244395.

4. M. Pompili, S. L. N. Hermans, S. Baier, et al., "Realization of a Multinode Quantum Network of Remote Solid-State Qubits," *Science* 372, no. 6539 (2021): 259–264, https://doi.org/10.1126/science.abe8798.

5. H. Huang, O. Alkhazragi, D. Liang, and F. Grillot, "Future Roles of Solid-State Quantum Dot Light Sources," *Applied Physics Letters* 126, no. 8 (2025): 080501, https://doi.org/10.1063/5.0251447.

6. C.-Y. Lu and J.-W. Pan, "Quantum-Dot Single-Photon Sources for the Quantum Internet," *Nature Nanotechnology* 16, no. 12 (2021): 1294–1296, https://doi.org/10.1038/s41565-021-01033-9.

7. Y.-R. Fan, Y. Luo, K. Guo, et al., "Quantum Entanglement Network Enabled by a State-Multiplexing Quantum Light Source," *Light: Science & Applications* 14 (2025): 189, https://doi.org/10.1038/s41377-025-01805-1, Open access.

8. A. Anwar, C. Perumangatt, A. Villar, A. Lohrmann, and A. Ling, "Development of Compact Entangled Photon-Pair Sources for Satellites," *Applied Physics Letters* 121, no. 22 (2022): 220503, https://doi.org/10.1063/5.0109702.

9. T. Kouadou, C. P. Lualdi, S. Johnson, et al., "Compact Entanglement Sources for Portable Quantum Information Platforms," in *Quantum Computing, Communication, and Simulation II*, Vol 12015 of *Proceedings of SPIE* (SPIE, 2022), 120150D.

10. S. Singh, F. Gu, S. de Bone, E. Villase nor, D. Elkouss, and J. Borregaard, "Modular Architectures and Entanglement Schemes for Error-Corrected Distributed Quantum Computation," *npj Quantum Information* (2025), https://doi.org/10.1038/s41534-025-01146-2.

11. Y.-A. Chen, Q. Zhang, T.-Y. Chen, et al., "An Integrated Space-to-Ground Quantum Communication Network over 4,600 Kilometres," *Nature* 589, no. 7841 (2021): 214–219, https://doi.org/10.1038/s41586-020-03093-8.

12. A. Conrad, S. Isaac, R. Cochran, et al., "Drone-Based Quantum Communication Links," in *Quantum Computing, Communication, and Simulation III*, Vol 12446 of *Proceedings of SPIE* (SPIE, 2023), 124460H.

13. J. Wang, J. Hanel, Z. Jiang, et al., "Time-Bin Encoded Quantum Key Distribution over 120 km with a Telecom Quantum Dot Source," *Light: Science & Applications* 15, no. 1 (2026): 126, https://doi.org/10.1038/s41377-026-02205-9.

14. C. Zhang, Y.-F. Huang, B.-H. Liu, C.-F. Li, and G.-C. Guo, "Spontaneous Parametric Down-Conversion Sources for Multiphoton Experiments," *Advanced Quantum Technologies* 4, no. 5 (2021): 2000132, https://doi.org/10.1002/qute.202000132.

15. N. Somaschi, V. Giesz, L. De Santis, et al., "Near-Optimal Single-Photon Sources in the Solid State," *Nature Photonics* 10, no. 5 (2016): 340–345, https://doi.org/10.1038/nphoton.2016.23.

16. H. Snijders, J. A. Frey, J. Norman, et al., "Fiber-Coupled Cavity-QED Source of Identical Single Photons," *Physical Review Applied* 9 (2021): 031002, https://doi.org/10.1103/PhysRevApplied.9.031002.

17. A. Musiał, K. Zołnacz, N. Srocka, et al., "Plug&Play Fiber-Coupled 73 kHz Single-Photon Source Operating in the Telecom O-Band," *Advanced Quantum Technologies* 3, no. 6 (2020): 2000018, https://doi.org/10.1002/qute.202000018.

18. N. Tomm, A. Javadi, N. O. Antoniadis, et al., "A Bright and Fast Source of Coherent Single Photons," *Nature Nanotechnology* 16, no. 4 (2021): 399–403, https://doi.org/10.1038/s41565-020-00831-x.

19. D. B. Northeast, D. Dalacu, J. F. Weber, et al., "Optical Fibre-Based Single Photon Source Using InAsP Quantum Dot Nanowires and Gradient-Index Lens Collection," *Scientific Reports* 11, no. 1 (2021): 22878, https://doi.org/10.1038/s41598-021-02287-y.

20. L. Rickert, K. Zołnacz, D. A. Vajner, et al., "A Fiber-Pigtailed Quantum Dot Device Generating Indistinguishable Photons at GHz Clock-Rates," *Nanophotonics* 14 (2025): 1795–1808, https://doi.org/10.1515/nanoph-2024-0519.

21. T. Gao, L. Rickert, F. Urban, et al., "A Quantum Key Distribution Testbed Using a Plug&Play Telecom-Wavelength Single-Photon Source," *Applied Physics Reviews* 9, no. 1 (2022), https://doi.org/10.1063/5.0070966.

22. R. Liu, G. G. Rozenman, N. K. Kundu, D. Chandra, and D. De, "Towards the Industrialisation of Quantum Key Distribution in Commu-





25119044, 2026, 10, Downloaded from https://advanced.onlinelibrary.wiley.com/doi/10.1002/qute.70510 by Universitatsbibliothek Stuttgart, Wiley Online Library on [02/11/2026]. See the Terms and Conditions (https://onlinelibrary.wiley.com/terms-and-conditions) on Wiley Online Library for rules of use; OA articles are governed by the applicable Creative Commons License

nication Networks: A Short Survey," *IET Quantum Communication* 3, no. 3 (2022): 151–163, https://doi.org/10.1049/qtc2.12044.

23. Z. Zhang, C. You, O. S. Maga na-Loaiza, et al., "Entanglement-Based Quantum Information Technology," *Advances in Optics and Photonics* 16, no. 1 (2023): 60–162, https://doi.org/10.1364/AOP.497143.

24. J. Yang, Z. Jiang, F. Benthin, et al., "High-Rate Intercity Quantum Key Distribution with a Semiconductor Single-Photon Source," *Light: Science & Applications* 13, no. 1 (2024): 150, https://doi.org/10.1038/s41377-024-01488-0.

25. J. Wang, P. Li, L. Sun, et al., "A Compact and Robust Polarization-Entangled Photon Source Towards Application in Mobile Platforms," *Photonics* 13, no. 2, (2026): 184, https://doi.org/10.3390/photonics13020184.

26. D. Kim, S. E. Economou, S. C. Bădescu, et al., "Optical Spin Initialization and Nondestructive Measurement in a Quantum Dot Molecule," *Physical Review Letters* 101 (2008): 236804, https://doi.org/10.1103/PhysRevLett.101.236804.

27. A. Ac'in, I. Bloch, H. Buhrman, et al., "The Quantum Technologies Roadmap: A European Community View," *New Journal of Physics* 20, no. 8 (2018): 080201, https://doi.org/10.1088/1367-2630/aad1ea.

28. P. van Loock, W. Alt, C. Becher, et al., "Extending Quantum Links: Modules for Fiber- and Memory-Based Quantum Repeaters," *Advanced Quantum Technologies* 3, no. 11 (2020): 1900141, https://doi.org/10.1002/qute.201900141.

29. C. Schimpf, M. Reindl, F. Basso Basset, K. D. Jöns, R. Trotta, and A. Rastelli, "Quantum Dots as Potential Sources of Strongly Entangled Photons: Perspectives and Challenges for Applications in Quantum Networks," *Applied Physics Letters* 118, no. 10 (2021): 100502, https://doi.org/10.1063/5.0038729.

30. S. Bounouar, M. Müller, A. M. Barth, M. Glässl, V. M. Axt, and P. Michler, "Phonon-Assisted Robust and Deterministic Two-Photon Biexciton Preparation in a Quantum Dot," *Physical Review B* 91 (2015): 161302, https://doi.org/10.1103/PhysRevB.91.161302.

31. Y. Chen, M. Zopf, R. Keil, F. Ding, and O. G. Schmidt, "Highly-Efficient Extraction of Entangled Photons from Quantum Dots Using a Broadband Optical Antenna," *Nature Communications* 9, no. 1 (2018): 2994, https://doi.org/10.1038/s41467-018-05456-2.

32. H. Wang, H. Hu, T.-H. Chung, et al., "On-Demand Semiconductor Source of Entangled Photons Which Simultaneously Has High Fidelity, Efficiency, and Indistinguishability," *Physical Review Letters* 122 (2019): 113602, https://doi.org/10.1103/PhysRevLett.122.113602.

33. J. Liu, R. Su, Y. Wei, et al., "A Solid-State Source of Strongly Entangled Photon Pairs with High Brightness and Indistinguishability," *Nature Nanotechnology* 14, no. 6 (2019): 586–593, https://doi.org/10.1038/s41565-019-0435-9.

34. C. Hopfmann, W. Nie, N. L. Sharma, C. Weigelt, F. Ding, and O. G. Schmidt, "Maximally Entangled and Gigahertz-Clocked On-Demand Photon Pair Source," *Physical Review B* 103 (2021): 075413, https://doi.org/10.1103/PhysRevB.103.075413.

35. R. Li, F. Liu, and Q. Lu, "Quantum Light Source Based on Semiconductor Quantum Dots: A Review," *Photonics* 10, no. 6 (2023), https://doi.org/10.3390/photonics10060639.

36. T. Strobel, S. Kazmaier, T. Bauer, et al., "High-Fidelity Distribution of Triggered Polarization-Entangled Telecom Photons via a 36 km Intra-City Fiber Network," *Optica Quantum* 2, no. 4 (2024): 274–281, https://doi.org/10.1364/OPTICAQ.530838.

37. Y. G. Zena, M. Pal, M. Langer, et al., "Enhanced Emission of GaAs Quantum Dots in Bend Nanomembranes," in *Quantum Communications and Quantum Imaging XXIII*, Vol 13618 (SPIE, 2025), 136180J.

38. M. Langer, S. A. Dhurjati, Y. G. Zena, et al., "Bright Quantum Dot Light Sources Using Monolithic Microlenses on Gold Back-Reflectors," *Nanotechnology* 36, no. 225301 (2025): 13, https://doi.org/10.1088/1361-6528/add350.

39. M. D. Eisaman, J. Fan, A. Migdall, and S. V. Polyakov, "Invited Review Article: Single-Photon Sources and Detectors," *Review of Scientific Instruments* 82, no. 7 (2011): 071101, https://doi.org/10.1063/1.3610677.

40. P. Sibson, J. E. Kennard, S. Stanisic, C. Erven, J. L. O'Brien, and M. G. Thompson, "Integrated Silicon Photonics for High-Speed Quantum Key Distribution," *Optica* 4, no. 2 (2017): 172, https://doi.org/10.1364/optica.4.000172.

41. D. A. Vajner, L. Rickert, T. Gao, K. Kaymazlar, and T. Heindel, "Quantum Communication Using Semiconductor Quantum Dots," *Advanced Quantum Technologies* 5, no. 7 (2022): 2100116, https://doi.org/10.1002/qute.202100116.

42. D. Huber, M. Reindl, Y. Huo, et al., "Highly Indistinguishable and Strongly Entangled Photons from Symmetric GaAs Quantum Dots," *Nature Communications* 8, no. 1 (2017): 15506, https://doi.org/10.1038/ncomms15506, Open access.

43. N. Margaria, F. Pastier, T. Bennour, et al., "Efficient Fibre-Pigtailed Source of Indistinguishable Single Photons," *Nature Communications* 16, no. 1 (2025): 7553, https://doi.org/10.1038/s41467-025-62712-y.

44. G. Shooter, Z.-H. Xiang, J. R. A. Müller, et al., "1GHz Clocked Distribution of Electrically Generated Entangled Photon Pairs," *Optics Express* 28, no. 24 (2020): 36838–36848, https://doi.org/10.1364/OE.405466.

45. L. Bremer, K. Weber, S. Fischbach, et al., "Quantum Dot Single-Photon Emission Coupled into Single-Mode Fibers with 3D Printed Micro-Objectives," *APL Photonics* 5, no. 10 (2020): 106101, https://doi.org/10.1063/5.0014921.

46. M. Langer, P. Ruchka, A. Rahimi, et al., "An Ultra-Compact Deterministic Source of Maximally Entangled Photon Pairs," *APL Photonics* 10, no. 6 (2025): 066117, https://doi.org/10.1063/5.0271023.

47. N. Tran, P. Ruchka, S. Jakovljevic, et al., "Collecting Telecom Photons From Circular Bragg Gratings Using Optical Fibers and 3D Printed Micro-Lenses," *Advanced Quantum Technologies* 8 (2025): e00450, https://doi.org/10.1002/qute.202500450, Open access under Creative Commons Attribution License.

48. A. N. Craddock, A. Lazenby, G. B. Portmann, R. Sekelsky, M. Flament, and M. Namazi, "Automated Distribution of Polarization-Entangled Photons Using Deployed New York City Fibers," *PRX Quantum* 5 (2024): 030330, https://doi.org/10.1103/PRXQuantum.5.030330.

49. J.-W. Pan, Z.-B. Chen, C.-Y. Lu, H. Weinfurter, A. Zeilinger, and M. Żukowski, "Multiphoton Entanglement and Interferometry," *Reviews of Modern Physics* 84 (2012): 777–838, https://doi.org/10.1103/RevModPhys.84.777.

50. P. Michler (Ed.), *Single Quantum Dots, Fundamentals, Applications, and New Concepts* (Springer, 2003).

51. C. Heyn, A. Stemmann, A. Schramm, H. Welsch, W. Hansen, and A. Nemcsics, "Faceting During GaAs Quantum Dot Self-Assembly by Droplet Epitaxy," *Applied Physics Letters* 90, no. 20 (2007): 203105, https://doi.org/10.1063/1.2737123.

52. Y. H. Huo, A. Rastelli, and O. G. Schmidt, "Ultra-Small Excitonic Fine Structure Splitting in Highly Symmetric Quantum Dots on GaAs (001) Substrate," *Applied Physics Letters* 102, no. 15 (2013): 152105, https://doi.org/10.1063/1.4802088.

53. R. Keil, M. Zopf, Y. Chen, et al., "Solid-State Ensemble of Highly Entangled Photon Sources at Rubidium Atomic Transitions," *Applied Physics Letters* 8, no. 1 (2017): 1–8.

54. A. Schlehahn, S. Fischbach, R. Schmidt, et al., "A Stand-Alone Fiber-Coupled Single-Photon Source," *Scientific Reports* 8, no. 1 (2018): 1340, https://doi.org/10.1038/s41598-017-19049-4.

55. M. Sartison, K. Weber, S. Thiele, et al., "3D-Printed Micro-Optics for Quantum Technology: Optimised Coupling of Single Quantum Dot Emission into a Single-Mode Fibre," *Light: Advanced Manufacturing* 2, no. LAM2020060010 (2021): 103, https://doi.org/10.37188/lam.2021.006.

56. L. Bremer, S. Rodt, and S. Reitzenstein, "Fiber-Coupled Quantum Light Sources Based on Solid-State Quantum Emitters," *Materials for*



25119044, 2026, 10, Downloaded from https://advanced.onlinelibrary.wiley.com/doi/10.1002/qute.70510 by Universitatsbibliothek Stuttgart, Wiley Online Library on [02/11/2026]. See the Terms and Conditions (https://onlinelibrary.wiley.com/terms-and-conditions) on Wiley Online Library for rules of use; OA articles are governed by the applicable Creative Commons License

*Quantum Technology* 2 (2022): 042002, https://doi.org/10.1088/2633-4356/aca3f3.

57. S. Stufler, P. Machnikowski, P. Ester, et al., "Two-Photon Rabi Oscillations in a Single $In_xGa_{1-x}As$/GaAs Quantum Dot," *Physical Review B* 73 (2006): 125304, https://doi.org/10.1103/PhysRevB.73.125304.

58. R. Winik, D. Cogan, Y. Don, et al., "On-Demand Source of Maximally Entangled Photon Pairs Using the Biexciton-Exciton Radiative Cascade," *Physical Review B* 95 (2017): 235435, https://doi.org/10.1103/PhysRevB.95.235435.

59. A. V. Kuhlmann, J. Houel, A. Ludwig, et al., "Charge Noise and Spin Noise in a Semiconductor Quantum Device," *Nature Physics* 9, no. 9 (2013): 570–575, https://doi.org/10.1038/nphys2688.

60. J. Yang, T. Fandrich, F. Benthin, et al., "Photoneutralization of Charges in GaAs Quantum Dot Based Entangled Photon Emitters," *Physical Review B* 105 (Mar 2022): 115301, https://doi.org/10.1103/PhysRevB.105.115301.

61. C. Hopfmann, N. L. Sharma, W. Nie, R. Keil, F. Ding, and O. G. Schmidt, "Heralded Preparation of Spin Qubits in Droplet-Etched GaAs Quantum Dots Using Quasiresonant Excitation," *Physical Review B* 104 (2021): 075301, https://doi.org/10.1103/PhysRevB.104.075301.

62. M. Reindl, K. D. Jöns, D. Huber, et al., "Phonon-Assisted Two-Photon Interference from Remote Quantum Emitters," *Nano Letters* 17, no. 7 (2017): 4090–4095, https://doi.org/10.1021/acs.nanolett.7b00777.

63. D. F. V. James, P. G. Kwiat, W. J. Munro, and A. G. White, "Measurement of Qubits," *Physical Review A* 64 (2001): 052312, https://doi.org/10.1103/PhysRevA.64.052312.

## Supporting Information

Additional supporting information can be found online in the Supporting Information section.

**Supporting File:** qute70510-sup-0001-SuppMat.pdf.



25119044, 2026, 10, Downloaded from https://advanced.onlinelibrary.wiley.com/doi/10.1002/qute.70510 by Universitatsbibliothek Stuttgart, Wiley Online Library on [02/11/2026]. See the Terms and Conditions (https://onlinelibrary.wiley.com/terms-and-conditions) on Wiley Online Library for rules of use; OA articles are governed by the applicable Creative Commons License